Drop shapes emerging at very low flow rates from thick-walled cylinders

A. López-Villa and A. Medina
SEPI ESIME Azcapotzalco, Instituto Politécnico Nacional,
Av. de las Granjas 682, Col. Santa Catarina, 02250, Azcapotzalco D.F., México.

C. A. Vargas
Laboratorio de Sistemas Complejos, Departamento de Ciencias Básicas, Universidad Autónoma Metropolitana Azcapotzalco,
Av. San Pablo 180, México D.F., 02200 México.

S. López and C. Duran
Instituto Mexicano del petróleo,
Eje Central Lázaro Cárdenas 152, Col. San Bartolo Atepehuacan, México D.F. 07730 México.

Recibido el 30 de junio de 2011; aceptado el 30 de noviembre de 2011

In this work we study the equilibrium shapes of drops that emerge slowly outside of vertical, thick-walled tubes. For low flow rates it is possible to calculate drop shapes by using the balance equation between the hydrostatic and injection and capillary pressures. Through the use of image processing software were obtained the center of mass and volume of the experimental drops and the qualitative agreement between our experimental and theoretical results is very good.

Keywords: Drops; capillary effects; interaction with surfaces.

En este trabajo se estudia las formas de equilibrio de gotas que emergen lentamente de tubos de pared gruesa. Para gastos bajos es posible calcular la forma de las gotas usando la ecuación de balance entre la presión hidrostática y la presión de inyección con la presión capilar. A través del uso de software de procesamiento de imágenes se obtienen resultados del centro de masa y el volumen de las gotas experimentales y se encuentra una gran concordancia con los resultados teóricos.

Descriptores: Gota; efectos capilares; interacción con superficies.

PACS: 47.55.D-; 47.55.nb; 47.55.dr

1. Introduction

The drop formation is a very common phenomenon in different branches of industry and its study has important practical consequences. Drop formation represents a basic phenomenon important in a wide variety of industrial and natural processes. For instance, all spraying processes, dispersing of pesticides, ink-jet printing and iron industry rely on controlling drop sizes and contact angle for efficient application. In the bibliography, two hydrodynamic mechanisms of drop formation are known: Surface tension always causes the breakup and is countered by the inertia of the liquid. [1–3]. The characterization of the drop shapes can be used to quantify important properties such as surface tension, σ [2, 4, 5], or the static contact angle, θ, formed between the inner liquid and the substrate surface [1, 6]. In a general case the liquid may has a good wetting when $\theta < \pi/2$ and it has a poor wetting when $\theta \geq \pi/2$, here we will analyze the drop shape for both cases (see Fig. 1) [1–3, 7].

One of the main motivations for considering the formation of drops in thick-walled tubes is the case where the degree of wetting of the primary slag on the walls of a blast furnace can change depending on the concentration of alumina and iron oxides [3]. For example, in Fig. 1 shown in the upper picture a drop of molten slag in a Mullite tube, in this case the slag contains a mass of 0% iron oxides (poor wetting), the slag drop in the lower picture contains a mass of 33% iron oxides (good wetting). In both cases the inner radius of the tube was a = 2.0 mm, the outer radius of the tube was R=8.5 mm, and finally the tube wall thickness was δ = 6.5 mm. The experimentation in this type of system is expensive and complex, but, in this work, detailed knowledge of the experimental shapes by means of theoretical calculations give reliable results and avoids performing expensive experiments.

This paper presents a theoretical and experimental study of equilibrium shapes of liquid axisymmetric drops which emerge from the thick-walled tube, for low flow rates, Q. This method allows the exact calculation of the characteristics drop shapes during their slow formation in ideal conditions. The flow rate is so low that a new form of drop formed with an angle θ does not depend on the shape of another formed with the angle $\theta + \Delta\theta$ or $\theta - \Delta\theta$. Formally, for a viscous fluid, the condition of low flow rate in the drop formation, can be expressed as the case where the capillary number, Ca, obeys $Ca \to 0$. The capillary number is a measure of the magnitude of viscous forces to the surface tension forces and it is written as $Ca = \mu Q/\sigma a^2$, where μ is the dynamic viscosity of the liquid and a is the inner radius of the tube through which the fluid was injected. When the liquid of density ρ, is considered inviscid fluid the dimensionless flow rate is expressed in terms of the Weber number, $We = \rho Q^2/\sigma a^3$, the Weber number is the ratio of kinetic forces to surface tension forces. In this case the condition of low flow rate occurs when $We \to 0$.

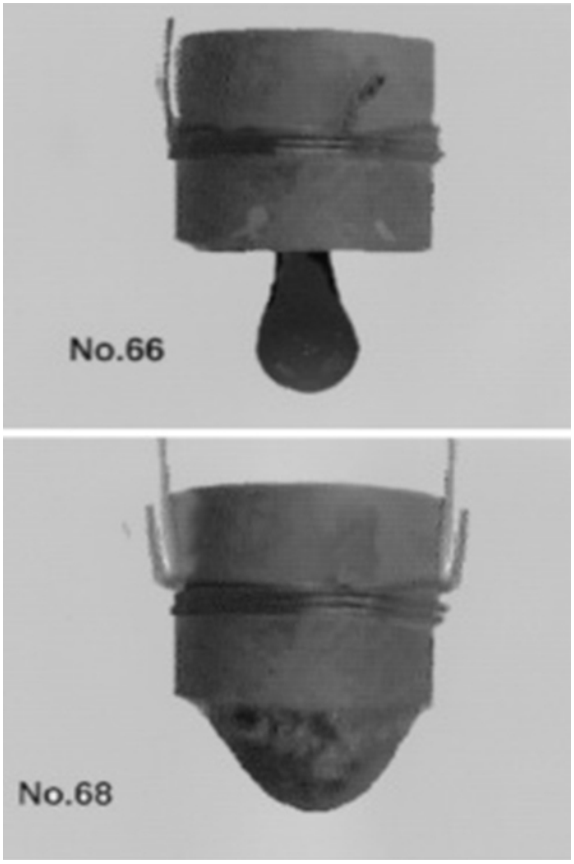

FIGURE 1. Picture of two drops of molten slag in a Mullite tube, in the upper photo the slag contains a mass of 0% iron oxide (poor wetting) in the lower picture it contains a mass of 33% iron oxide (good wetting).

It is important to note the cases where the formation of drops at high flow rates and the jets formation [1, 8, 9], will not be considered in this work. It is also important to note that the analysis of the "pinch singularity" of the drop, is beyond the scope of this work.

Here are discussed through experiments, various features of the shape drops in function of the Bond number, $Bo = \rho g R^2/\sigma$, where g is the gravity acceleration and R is the outer radius of the tube. The Bond number is the ratio of the hydrostatic pressure to the capillary pressure (the ratio of gravitational forces to capillary forces). If $Bo > 1$, dominates the gravitational force on the capillary ones, while if $Bo < 1$, dominates the capillary force. In the quasi-static regime the study of the drop shapes is very similar to that of bubbles [6, 10–15], therefore θ plays an important role in the drops formation, as it is well known to happen in bubbles formation [16].

There is little work related to the problem of drop shape when it emerges from thick-walled tubes, the study is of form quasi-static [17], *i.e.* it assume that $We \to 0$ in the non viscous case.

The angle that takes the drop as it emerges from the top of a tube and reaches the edge of this is the static contact angle, however, increases in injection pressure leads to this angle may increase to a maximum value $\theta + \pi/2$ just before breaking, this case is discussed here through experiments. It does not happen in the case of a drop that emerges in the direction of the gravity force. When the drop emerges from below the value of the angle do not change, this will be discussed later in this work. The qualitative agreement between our experimental and theoretical results is very good.

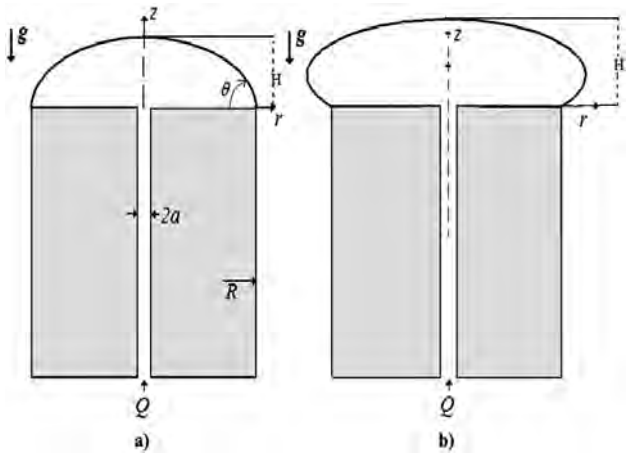

FIGURE 2. Schematie of the drop shape emerging in a thick walled tube: (a) drop with good wetting (contact angle $< \pi/2$) and (b) drop with poor wetting (contact angle $> \pi/2$).

For our purpose the division of this paper is; in the next section the problem and the equations for the free surface was formulated in dimensionless form and in the Sec. 3 are discussed the experiments performed to verify the existing theoretical results. In the Sec. 4 the main conclusions and results of this study are given.

2. Problem Formulation

We consider that a drop emerges, on the top or the bottom of a vertical thick-walled tube. The drop is generated at a very low flow rate so that, the drop shape can be described by an equation of balance between the hydrostatic and injection pressure and capillary pressure, *i.e.*, in this conditions the drop remains in equilibrium and with the same shape. In this case the description of the drop shape can be made by using the Young-Laplace equation [1, 2, 7, 10, 11].

A scheme of the problem of slow injection (quasi-static case) of a liquid in a thick-walled cylinder of inner radius a and outer radius $R = a + d$ is shown in Fig. 2. On the drop surface the capillary pressure, p_c, must be equal to the sum of the liquid injection pressure, p_0, hydrostatic pressure, $\rho g z$, and the atmospheric pressure, p_a [1], *i.e.*,

$$p_c = p_0 - \rho g z - p_a. \tag{1}$$

Note that the injection pressure, must be greater than the hydrostatic pressure , *i.e.*, $p_0 > \rho g z$ when the drop emerges at the top tube, if it emerges at the bottom tube these pressures are added. The use of this condition allows the growth drop.

Since equation $p_c = \sigma \nabla \cdot \mathbf{n}$ [18,19], where $\mathbf{n}$ is a normal unit vector to the outer drop surface, and with $P = p_0 - p_a$, if

$$\nabla \cdot \mathbf{n} = \left(\frac{1}{R_1} + \frac{1}{R_2} \right), \tag{2}$$

where R_1 and R_2 are the radii of curvature.

We have that the dimensionless differential equation for the free surface in cylindrical coordinates [1], is

$$- \frac{\frac{d^2\xi}{d\zeta^2}}{Bo\left[\left(\frac{H}{R}\right)^2 + \left(\frac{d\xi}{d\zeta}\right)^2\right]^{3/2}} + \frac{1}{Bo\xi\left[\left(\frac{H}{R}\right)^2 + \left(\frac{d\xi}{d\zeta}\right)^2\right]^{1/2}} = p - \zeta, \tag{3}$$

were $\xi = r/R$, $\zeta = z/H$ and $p = P/\rho g H$. R is the outer radius and H is the maximum drop height. The dimensionless boundary conditions are

$$\begin{aligned} &\text{at} \quad \zeta = 1 : \xi = 0 \quad \text{and} \quad \frac{d\xi}{d\zeta} \to \infty, \\ &\text{at} \quad \zeta = 0 : \xi = 1 \quad \text{and} \quad \frac{d\xi}{d\zeta} = \tan\theta, \end{aligned} \tag{4}$$

and the dimensionless volume takes the form

$$\int_0^1 \xi^2(\zeta) d\zeta = \frac{V}{\pi R^3}. \tag{5}$$

It should be noted that the static contact angle values are in the range $[\theta, \pi/2 + \theta]$ [17], the maximum angle is caused by the injection pressure and takes this value just before break of the drop.

Equation (3) is a highly nonlinear differential equation. In the next section we present their solutions in some cases of interest. The intention of the experiments is to prove that Eq. (3) allows to calculate θ, ρ and σ. This is achieved if we have two values and the third one is to be calculated.

3. Results and Discussion

In this section we discuss experiments and qualitatively compare the experimental drop profiles to the theoretical shapes. The experiments were performed using steel, silver and plastic tubes and, water, silicone oil of different viscosities, transmission oil and mercury as working fluids.

The slow growth of the drops was achieved by injecting liquid through a hose connected to it with a liquid level just above of the tube output. This method is suitable for the drops formed from up or down.

The experiments were video recordered with a high speed video camera model REDLAKE MotionXtra HG-100K, from video images may also have the drop evolution, from its formation to the "pinch singularity", but we are only interested in the equilibrium drop shapes.

4. Solutions

4.1. Solution for the case Bo$\ll$1

An important case of drop formation with analytical solution of Eq. (3) occurs when $Bo \ll 1$, *i.e.*, the capillary effects dominate over the gravitational. In this case the resulting differential equation, obtained from Eq. (3), is

$$\frac{d^2\xi}{d\zeta^2} = \frac{1}{\xi}\left[\left(\frac{H}{R}\right)^2 + \left(\frac{d\xi}{d\zeta}\right)^2\right], \tag{6}$$

the solutions of this equation, with boundary conditions (4), are spheres

$$\xi = \sqrt{(\frac{H}{R} - \tan\alpha)^2 - (\zeta - \tan\alpha)^2}, \tag{7}$$

where $\alpha = \theta - \pi/2$.

When the effect of gravity is neglected the drop volume can be obtained from Eq. (7) and (6). It gives

$$V = \frac{1}{3}\frac{(1+\sin\alpha)^2(2-\sin\alpha)}{\cos^3\alpha}, \tag{8}$$

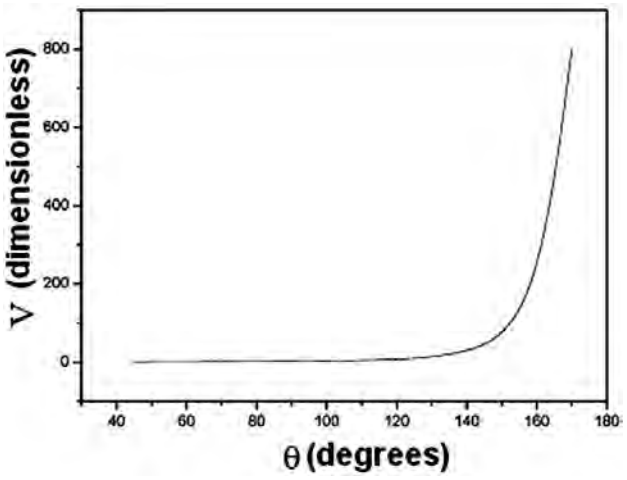

FIGURE 3. Dimensionless maximum volume of a spherical drop as a contact angle function.

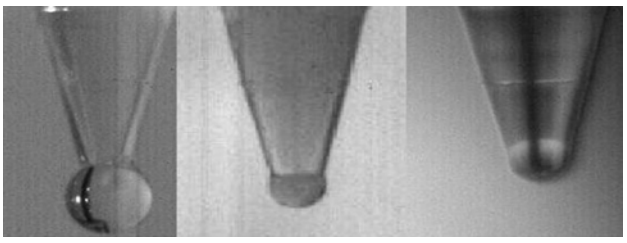

FIGURE 4. Experimental profiles of spherical drops from poor and good wetting.

where V is the dimensionless volume. Figure 3 shows the plot of V as a function of θ. Figure 3 is shown that the dimensionless drop volume grows significantly when the contact angle increases, *i.e.*, when $\theta \to 180°$, $V \to \infty$ this compares with previous results as [17].

Figure 4 shows that the experimental profiles of three drops in case of poor and good wetting, are spherical sections, the poor wetting case is made with water and plastic and the good one is with silicone oil and plastic. In these cases the Bond number value is small. In the poor wetting case, Bo =0.0053 and in the good one case, Bo =0.018, and the condition that liquid emerges from above or below does not play an important role, during the experiment, the orientation is neglected. The Bond number for small radii are also small see Fig. 5. Note that the Bond number does not appear explicitly in the solution (7). The Bond numbers used in the experiments in Fig. 4 are very small and the drops are sphere sections, where the volumes are determined by the contact angle, in these cases $\theta = 130°$ and $\theta = 110°$ for the poor wetting case and $\theta = 30°$ for the good wetting case.

substance	ρ (Kg/m³)	σ (N/m)	r (m)	Bo
distilled water	1000	0.0728	0.00095	0.1216
silicone oil 10	960	0.0208	0.00095	0.4085
silicone oil 1000	971	0.0212	0.00095	0.4055
distilled water	1000	0.0728	0.04	215.4
Mercury	13,529	0.465	0.00165	0.77
silicone oil 1000	971	0.0212	0.024	258.5
distilled water	1000	0.0728	0.0002	0.0053
silicone oil 1000	971	0.0212	0.0002	0.018

FIGURE 5. Table of materials and data used in experiments.

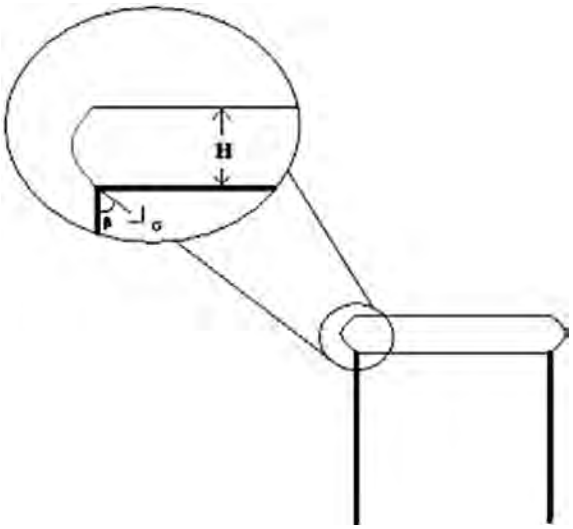

FIGURE 6. Enlargement of a drop that emerges on top tube with $B_0 \gg 1$

4.2. Solution for Bo≫1 and H/R≪1

Other case of interest is when $Bo \gg 1$, *i.e.*, the gravitational effects dominate over the capillary ones and $H/R \gg 1$ (the drop is flat). In this case the left hand side of Eq. (3) can be neglected and the resulting equation is

$$\zeta = p. \tag{9}$$

In the Ec. (9) describes the profile of a very flat dimensionless drop with height equal to the dimensionless pressure p. Figure 6 schematically shows the drop shape under these conditions. The approach to the edge of the drop profile define the important parameters in the analysis of the forces that deform the drop.

Figure 6 shows that a force, per unit length, acting on the drop is due to the hydrostatic pressure tends to expand laterally. Integrating this force from the base of the nozzle to the maximum drop height, H,

$$\int_0^H \rho g z dz = \frac{1}{2}\rho g H^2. \tag{10}$$

Because the drop profile is in equilibrium, this force must be equal to the force, per unit length, that limits the drop expansion. Such a force is $\sigma\cos\beta + \sigma$ (see Fig. 4). Where $\beta = \pi - \theta$ or $\beta = \theta$, respectively, for poor and good wetting. Finally, the forces balance gives us the equation

$$\frac{1}{2}\rho g H^2 = \sigma\cos\beta + \sigma, \tag{11}$$

the dimensionless equation for the equilibrium height is

$$\frac{H}{R} \sim 2\sqrt{\frac{\cos\beta + 1}{Bo}}. \tag{12}$$

Equation (12) we can see that the dimensionless height H/R is implicitly a function of angle θ and of the Bond number. We have $Bo \gg 1$ and $\cos\beta \leq 1$ then $H/R \ll 1$. This can be checked with high Bond number values and different

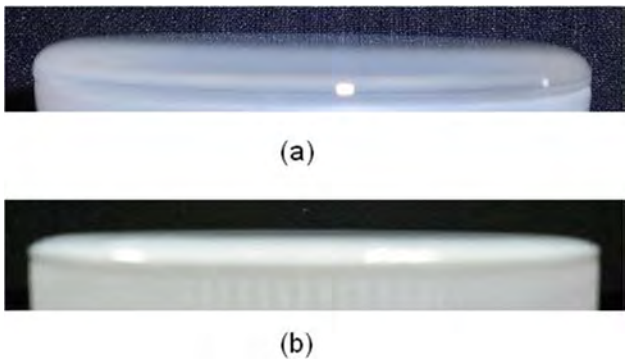

FIGURE 7. Picture of two flat drops with $B_0 \gg 1$ with two different contact angles.

contact angles. The experimental results are shown in Fig. 7 for cases of good and poor wetting, showing a picture with two cases of a drop emerging from a cylinder with large inner radius and with good and poor wetting, in the poor wetting case, the tube is plastic and the liquid is water and Bo =215.4, for good wetting was used a plastic tube and silicone oil and Bo =258.5.

When the Bond number is large the drop is flat and its maximum height H/R is small.

4.3. Solution for ($d\zeta/d\xi \ll$1 Small slopes)

In the case of good wetting, *i.e.* when the slope is small, $d\zeta/d\xi \ll 1$ and therefore $(d\zeta/d\xi)^2 \ll 1$.

To simplify the calculation, in the Eq. (3), for this case the dimensionless height ζ is a function of the radius ξ, under these new conditions the equation is

$$\frac{d^2\zeta}{d\xi^2} + \frac{1}{\xi}\frac{d\zeta}{d\xi} = Bo(p-\zeta), \tag{13}$$

where the boundary conditions are

$$\text{at} \quad \xi = 0 : \zeta = H/R \quad \text{and} \quad \frac{d\zeta}{d\xi} = 0, \tag{14}$$

$$\text{at} \quad \xi = 1 : \zeta = 0 \quad \text{and} \quad \frac{d\zeta}{d\xi} = \frac{1}{\tan\theta}\,. \tag{15}$$

The solution for the Eq. (13) is

$$\zeta(\xi) = pBo - \frac{1}{I_1(1)\tan\theta}(1 - I_0(\xi)), \tag{16}$$

where I_0, I_1 are respectively the modified Bessel functions of order zero and one. This solution corresponds to a drop emerging from the top of the tube.

For the case when the drop emerges from the bottom, the solution is

$$\zeta(\xi) = pBo - \frac{\tan\theta(J_0(\xi) - 1)}{J_1(1)}, \tag{17}$$

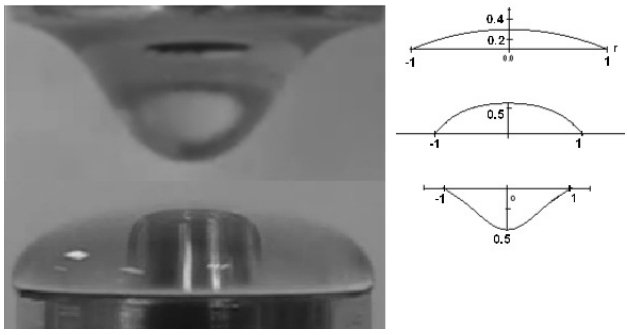

FIGURE 8. Drop profiles emerging from a tube, plotted from the Bessel solutions.

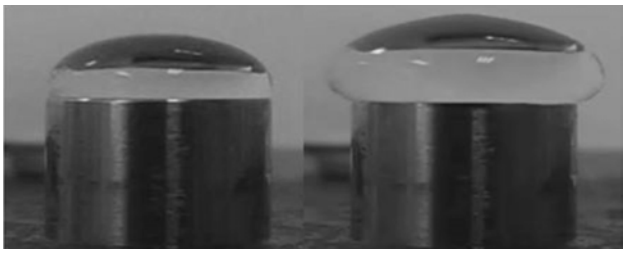

FIGURE 9. A picture of a drop in two equilibrium cases, where the contact angle varies between θ to $\theta + \pi/2$

where J_0 and J_1 Bessel functions of order zero and one, respectively. There are previous work with similar results, for different cases [1].

In Fig. 8, shows two profiles of drops emerging of the top (Eq. (16)) and a drop that emerges from the bottom (Eq. (17)), this shapes were plotted from the solutions of Bessel function, In the same figure it is shown the picture of two silicone oil drops emerging up and down in a steel tube, with $Bo = 0.4085$ and $\theta = 45°$ There is a good agreement for small slope with analytical solution.

5. Analysis of the general forms

A drop growing at a low flow rate is considered in equilibrium and the only way to grow is a change in the injection pressure. When the pressure changes, also change the drop equilibrium conditions, in this case the change in the drop volume is due to a change in the contact angle, which is possible to measure, and we know that the changes in angle are from θ to $\theta + \pi/2$ [17], figure 9 shows the case of a water drop emerging in a steel tube and it can be seen that the angle of the liquid with steel is $90°$ at the beginning and then grows to almost 180°, here Bo =0.1216.

On the other hand, water drop emerging down with the same conditions can be seen in Fig. 10, this case shows that the contact angle value does not change by varying the injection pressure, the volume changes until the surface tension permits. Analytical calculations given a good approximation of the experimental results.

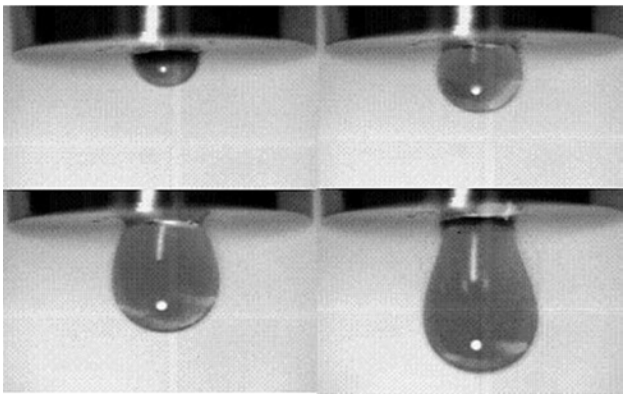

FIGURE 10. Series that shows the different equilibrium moments of a drop with poor wetting, growing from of bottom part of a tube.

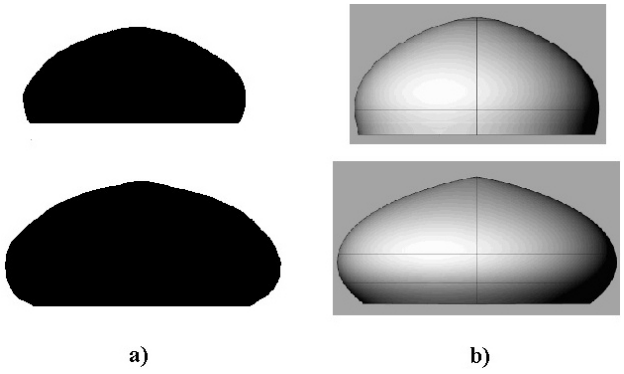

FIGURE 11. Figure showing how from the drop picture you can get the area and volume.

From the pictures taken from the experiments were followed up at the drops mass centers emerging from the top and below of the tube. The plots were made varying the injection pressure and thus the volume of the drop.

With commercial software the picture is brought to a drop of three-dimensional shape. Mastercam X4 and Rhinoceros were used for evolve volumes, see Fig. 11 where showing examples of the drops emerging from the top tube (Fig. 11a) to observe the shapes of black and white shapes (Fig. 11b) axisymmetric drop shapes. In the same way you do for bottom tube case.

With the use of the software above mentioned the mass center of the drops emerging on the edge bottom follow a curve similar to that of bubbles emerging up and with wall effect, these forms depend on the Bond number in both case. In Fig. 12 are shown the two cases, a) shows a bubble with Bo=0.04 and the effect of the walls of a cone with an angle of 15°, in Fig. 12b) is shown a drop with Bo=0.1216, the plot is drawing so that the center of mass was comparable with that of the bubble, *i.e.*, will change the direction of the axis.

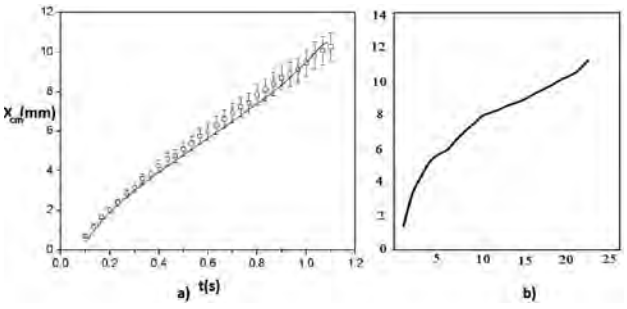

FIGURE 12. Mass center of a drop with poor wetting and growing downward compared with the bubble dynamic.

FIGURE 13. Comparison of two drop volumes, the drops grow with different boundary conditions on walls tube.

Finally we changed the boundary conditions on the walls, the tube does not end at an angle of 90°, instead we change of the angle to 135° and the drop volume increases as seen in Fig. 13, where the angle change achieved a remarkable change in height H and therefore a change in the drop volume. This is attributed to the sliding drop surface on the tube wall and it maintains the contact angle between θ and $\theta+\pi/2$, and also the volume is growing, does not contradict the condition for the angle is within this range.

6. Conclusions

In this paper we studied theoretically and experimentally, the drop shapes that emerge slowly from thick-walled tubes. In the first example, we gave the equation that models the drop shape and we show some solutions of this equation. It in several limits gives good approximations to the experiments presented in each case. Results of experiments describe the quasi-static drops shapes that emerge from thick-walled tubes, the shapes are retrieved from pictures taken from the experiments and then with the help of commercial software, we found the mass centers and drops volumes. Through various experiments we established that the drop shapes are heavily dependent on injection pressure, the contact angle and the Bond number. The experiments shown here describe qualitative and quantitatively the quasi-static drop shapes of the studied cases. An important result is that from the equation of the drop shape we have one of the parameters, given the other two, *i.e.*, you can get one of the three parameters θ, σ or ρ given two of them.

Acknowledgments

Authors acknowledge CONACyT-IPN by the Project of Equipment:"Laboratorio de Experimentación en Termofluidos", number CONACYT 124304, they also acknowledge to IPN for the partial support of this work through the project SIP 20110965 "Imbibición en espacios delgados complejos" and SIP 20113268, "Estudio del equilibrio y la estabilidad de espumas en tubos cónicos".

1. S. Middleman, *Modeling Axisymmetric Flows: Dynamics of Films*, Jets, and Drops (Academic Press, San Diego, 1995).
2. P.-G. de Gennes, F. Brochard-Wyart, and D. Quéré, *Capillarity and Wetting Phenomena: Drops, Bubbles, Pearls, Waves* (Springer, Berlin, 2004).
3. M. Hino, T. Nagasaka, A. Katsumata, K-I. Higuchi, K. Yamaguchi, and N. Kon-No, *Metall. Mater. Trans. B* **30** (1999) 671.
4. J. M. Andreas, S. E. A. Hauser, and W. B. Tucker, *J. Phys. Chem.* **42** (1938) 1001.
5. S. Fordham, *Proc. Roy. Soc. London, Series A* **194** (1948) 1.
6. P. D. Weidman, S. Krumdieck, and P. Rouse, *J. Fluid Mech.* **219** (1990) 25.
7. G. K. Batchelor, *An introduction to fluid dynamics* (Cambridge University Press, Cambridge, 2010).
8. M. R. Davidson, and J. J. Cooper-White, *Proceedings of the Third International Conference on CFD in Minerals and Process Industries* CSIRO, (Melbourne, Australia 2003).
9. P. Doshi *et al*., *Science* **302** (2003) 1185.
10. M.S. Longuet-Higgins, B.R. Kerman, K. Lunde, *J. Fluid Mech.* **230** (1990) 365.
11. D. Gerlach, G. Biswas, F. Durst and V. Kolobaric, *Int. J. Heat and Mass Tranfer* **48** (2005) 425.
12. N. Dietrich, S. Poncin, N. Midoux, and H. Z. Li, *Langmuir* **24** (2008) 13904.
13. M. Hino, T. Nagasaka, A. Katsumata, K-I. Higuchi, K. Yamaguchi, and N. Kon-No, *Metall. Mater. Trans. B* **30** (1999) 671.
14. C. Clanet and J. C. Lasheras, *J. Fluid Mech.* **383** (1999) 307.
15. J. Chatterjee, *J. Colloid Interface Scie.* **314** (2007) 199.
16. G. Corchero, A. Medina and F. J. Higuera, *Colloids and Surfaces A* **290** (2006) 41.
17. J. F. Oliver, C. Huh, and S. G. Mason, *J. Colloid Interface Scie.* **59** (1977) 568.
18. A. Liñan Martínez, M. Rodríguez Fernández, and F. J. Higuera Antón, *Mecánica de Fluidos* Lecciones 1 a 22, tercer curso (Madrid, Septiembre 2003).
19. L. D. Landau, E. M. Lifshitz, *Fluid Mechanics* (Pergamon Press, Londres, 1987).